Prognostic Modeling Studies of the Keweenaw Current in Lake Superior. Part I: Formation and Evolution

CHANGSHENG CHEN,* JIANRONG ZHU,+ ELISE RALPH,# SARAH A. GREEN,@ JUDITH WELLS BUDD,& AND FRANK Y. ZHANG**

* *Department of Marine Sciences, University of Georgia, Athens, Georgia*
+ *State Key Laboratory for Estuarine and Coastal Research, East China Normal University, Shanghai, China*
# *Great Lakes Observatory, University of Minnesota, Duluth, Minnesota*
@ *Department of Chemistry, Michigan Technological University, Houghton, Michigan*
& *Department of Geological Engineering and Sciences, Michigan Technological University, Houghton, Michigan*
** *Department of Biology, Kean University, Union, New Jersey*

(Manuscript received 5 February 1999, in final form 15 March 2000)

ABSTRACT

The formation and evolution of the Keweenaw Current in Lake Superior were examined using a nonorthogonal-coordinate primitive equation numerical model. The model was initialized by the monthly averaged temperature field observed in June and September 1973 and run prognostically under different forcing conditions with and without winds. As a Rossby adjustment problem, the model predicted the formation of a well-defined coastal current jet within an inertial period of 16.4 h after the current field adjusted to the initial temperature field. The magnitude and direction of this current jet varied with the cross-shelf temperature gradient and wind velocity. It tended to intensify during northeastward (downwelling favorable) winds, and to lessen, or even reverse, during southwestward to northwestward (upwelling favorable) or southeastward (downwelling favorable) winds. In a case with strong stratification and without external atmospheric forcings, a well-defined clockwise warm-core eddy formed near the northeastern coast of the Keweenaw Peninsula as a result of baroclinic instability. A warm-core eddy was detected recently from satellite surface temperature images, the shape and location of which were very similar to those of the model-predicted eddy. The energy budget analysis suggested that the eddy kinetic energy grew exponentially over a timescale of 7 days. Growth was due to a rapid energy transfer from available eddy potential energy. The subsequent decline of the eddy kinetic energy was the result of turbulent diffusion, transfer from the eddy kinetic energy to mean kinetic energy, and outward net energy flux.

1. Introduction

Lake Superior is one of the largest lakes in the world and contains almost 10% of the earth's total surface freshwater (Matheson and Munawar 1978). It occupies an area of about 82 000 km^2 and has a coastline of about 5000 km. The geometry of the lake is similar to that of a shallow oceanic basin with an average depth of 146 m and a maximum depth of 406 m (Fig. 1). The average slope of the shelf is about 0.01 on the northern coast and about 0.005–0.035 on the southern coast. The narrowest shelf is located along the Keweenaw Peninsula, where the slope exceeds 0.05.

The general circulation of Lake Superior is cyclonic. This circulation gyre is driven by northward or northeastward winds and a cross-shelf temperature gradient over the sloping bottom topography along the coast. Lake Superior is located at midlatitude where an eastward wind is dominant (Phillips 1978). A northeastward or southeastward wind, with an average speed of 8–15 m s^{-1}, prevails over 40% of a year. These winds tend to drive a southeastward or northeastward flow near the surface with a return flow near the bottom, resulting in a cyclonic, vertically averaged current around the lake. During summer and fall, the near-surface water temperature is generally higher near the coast and lower in the interior. A sharp decrease of the temperature usually occurs over the shelf, forming a cross-isobath thermal front (or thermal bar) around the coast. This front tends to produce an alongfrontal, geostrophic, buoyancy circulation with the warmer temperature on the right, intensifying the wind-driven cyclonic gyre around the lake.

The cyclonic current dramatically accelerates near the Keweenaw Peninsula along the southern shore of Lake Superior where the bottom slope is steep. Under northeastward wind conditions in summer and fall, the east-

Corresponding author address: Dr. Changsheng Chen, Dept. of Marine Sciences, University of Georgia, Athens, GA 30602.

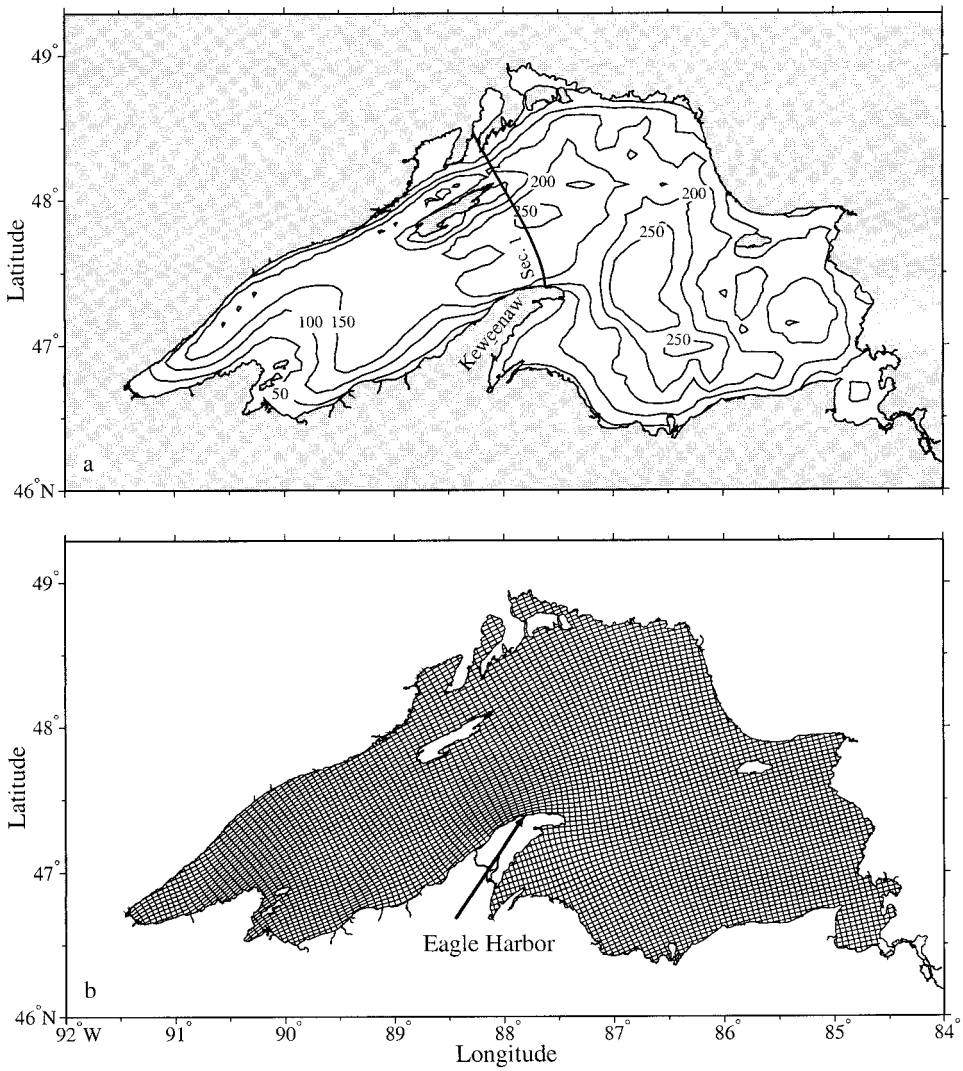

FIG. 1. Bottom topography (m) of Lake Superior (a) and numerical model grid (b). Heavy solid line represents the section used to present the cross-shelf distribution of temperature and currents in subsequent figures.

ward coastal current can exceed 60 cm s^{-1} (Niebauer et al. 1977); this strong current jet is known as the Keweenaw Current. The temporal variation of the Keweenaw Current is controlled mainly by synoptic and local atmospheric conditions associated with seasonal heating, atmospheric frontal passages, and local lake breezes. Increased solar heating in summer and fall tends to intensify the cross-shelf thermal front, and hence leads directly to the seasonal acceleration of the current jet. In summer, the wind field over Lake Superior is dominantly controlled by the atmospheric frontal passages with a timescale of 4–6 days. Correspondingly, the Keweenaw Current is usually a pulsating coastal jet with a period of about 5 days. The lake breeze is a diurnal fluctuation of the local surface wind field caused by the day–night reversal of the temperature gradient between the land and lake. This wind fluctuation plus diurnal heat flux tends to cause the short-term (daily) variation of the Keweenaw Current.

Several observational studies have been conducted to characterize the features of the Keweenaw Current and its relation to the thermal bar and winds Green and Yeske 1974; Ragotzkie 1974; Yeske and Green 1975; Diehl et al. 1977; Niebauer et al. 1977; Bennett 1978). Based on hydrographic, wind, and current measurements taken on a transect near Eagle Harbor in July 1973, Niebauer et al. (1977) first comprehensively described the wind- and buoyancy-driven nature of the Keweenaw Current. The current tended to accelerate as the thermal bar was pushed shoreward during a downwelling-favorable wind and to decelerate as the thermal bar was advected and diffused offshore during an upwelling wind.

The characteristics of the Keweenaw Current are very

similar to the alongshelf, buoyancy-driven current at a density front on a continental shelf in the ocean. Physical processes controlling its formation and evolution are identical to those found in the coastal ocean. Verifying and qualifying these processes will help us understand the formation and maintenance of the near-coastal jet current on the inner shelf of the ocean.

In the past two decades, no prognostic, primitive equation model experiments were conducted to study the Keweenaw Current. Previous modeling efforts were mainly based on some simplified barotropic or diagnostic models (e.g., Lam 1978). As a result, a successful simulation of the Keweenaw Current with realistic atmospheric forcing has not been accomplished. How does the Keweenaw Current vary with wind direction? Can the thermal bar become unstable and cause the formation of eddies along the Keweenaw coast? What is the physical mechanism responsible for the instability of the thermal bar? These questions have not been addressed in previous modeling studies.

A nonorthogonal coordinate transformation, primitive equation model has been applied to study the dynamics of the Keweenaw Current under the 1973 summertime hydrographic conditions. Special attention was paid to the physical processes that control the formation and evolution of the thermal front and Keweenaw Current during the summer. The linear theory of baroclinic instability and energy diagnostics were used to characterize the physical mechanisms responsible for eddy formation.

The remaining sections are organized as follows. The physical model and the design of numerical experiments are described in section 2. The model results of the density- and wind-induced circulation are presented in section 3. The baroclinic instability of the thermal front and eddy formation are examined in section 4. A summary is given in section 5.

2. Numerical model

The numerical model used in this study is a nonorthogonal coordinate transformation, primitive equation, coastal ocean circulation model developed by Chen et al. (1999, manuscript submitted to *J. Atmos. Oceanic Technol.*). This model was developed by modifying the Blumberg and Mellor model (the so-called ECOM-si, version Blumberg and Mellor 1987; Blumberg 1994). Removing the strict orthogonal restriction in ECOM-si, this model provides a proper fitting of the coastline and a fast convergence for grid generation. A detailed description of the nonorthogonal coordinate transformation model is given in Chen et al. and a brief description of the governing equations is given next.

In a horizontally nonorthogonal, and vertically stretched sigma-coordinate transformation system, the governing equations for momentum, water temperature, and density are given as

$$\frac{\partial DJu_1}{\partial t} + \frac{\partial DJ\hat{U}u_1}{\partial \xi} + \frac{\partial DJ\hat{V}u_1}{\partial \eta} + \frac{\partial J\omega u_1}{\partial \sigma} - Dh_2\hat{V}\left[v_1\frac{\partial}{\partial \xi}\left(\frac{J}{h_1}\right) - u_1\frac{\partial}{\partial \eta}\left(\frac{J}{h_2}\right) + Jf\right] - Dh_2u_1v_1\frac{\partial}{\partial \xi}\left(\frac{h_3}{h_1h_2}\right)$$
$$= -h_2gD\frac{\partial \zeta}{\partial \xi} + \frac{gh_2D}{\rho_o}\frac{\partial D}{\partial \xi}\int_\sigma^0 \sigma\frac{\partial \rho}{\partial \sigma}\,d\sigma - \frac{gh_2D^2}{\rho_o}\frac{\partial}{\partial \xi}\int_\sigma^0 \rho\,d\sigma + \frac{1}{D}\frac{\partial}{\partial \sigma}\left(K_m\frac{\partial Ju_1}{\partial \sigma}\right) + DJF_x \quad (1)$$

$$\frac{\partial DJv_1}{\partial t} + \frac{\partial DJ\hat{U}v_1}{\partial \xi} + \frac{\partial DJ\hat{V}v_1}{\partial \eta} + \frac{\partial J\omega v_1}{\partial \sigma} + Dh_1\hat{U}\left[v_1\frac{\partial}{\partial \xi}\left(\frac{J}{h_1}\right) - u_1\frac{\partial}{\partial \eta}\left(\frac{J}{h_2}\right) + Jf\right] - Dh_1u_1v_1\frac{\partial}{\partial \eta}\left(\frac{h_3}{h_1h_2}\right)$$
$$= -h_1gD\frac{\partial \zeta}{\partial \eta} + \frac{gh_1D}{\rho_o}\frac{\partial D}{\partial \eta}\int_\sigma^0 \sigma\frac{\partial \rho}{\partial \sigma}\,d\sigma - \frac{gh_1D^2}{\rho_o}\frac{\partial}{\partial \eta}\int_\sigma^0 \rho\,d\sigma + \frac{1}{D}\frac{\partial}{\partial \sigma}\left(K_m\frac{\partial Jv_1}{\partial \sigma}\right) + DJF_y \quad (2)$$

$$\frac{\partial \zeta}{\partial t} + \frac{1}{J}\left[\frac{\partial}{\partial \xi}(DJ\hat{U}) + \frac{\partial}{\partial \eta}(DJ\hat{V})\right] + \frac{\partial \omega}{\partial \sigma} = 0 \quad (3)$$

$$\frac{\partial JD\theta}{\partial t} + \frac{\partial JD\hat{U}\theta}{\partial \xi} + \frac{\partial JD\hat{V}\theta}{\partial \eta} + \frac{\partial J\omega\theta}{\partial \sigma} = \frac{1}{D}\frac{\partial}{\partial \sigma}\left(K_h\frac{\partial J\theta}{\partial \sigma}\right) + DJF_\theta \quad (4)$$

$$\rho_{\text{total}} = \rho_{\text{total}}(\theta, P), \quad (5)$$

where

$$\omega = w - \sigma\left(\hat{U}\frac{\partial D}{\partial \xi} + \hat{V}\frac{\partial D}{\partial \eta}\right) - \left[(1+\sigma)\frac{\partial \zeta}{\partial t} + \hat{U}\frac{\partial \zeta}{\partial \xi} + \hat{V}\frac{\partial \zeta}{\partial \eta}\right], \quad (6)$$

and ξ, η, and σ are defined as

$$\xi = \xi(x, y), \qquad \eta = \eta(x, y), \qquad \sigma = \frac{z - \zeta}{H + \zeta}. \quad (7)$$

Here σ varies from -1 at $z = -H$ to 0 at $z = \zeta$; x, y, and z are the eastward, northward, and upward axes of the orthogonal Cartesian coordinates; ζ is the surface elevation; H is the water depth; and u_1 and v_1 are the ξ and η components of the velocity that can be converted back to the x and y components (u and v) of the velocity using the relationship of

$$u_1 = \frac{h_2}{J}(x_\xi u + y_\xi v), \qquad v_1 = \frac{h_1}{J}(x_\eta u + y_\eta v), \quad (8)$$

where J is the Jacobian function with the form of $J = x_\xi y_\eta - x_\eta y_\xi$. The subscripts ξ and η indicate partial derivatives. The metric factors h_1 and h_2 of the coordinate transformation are defined as

$$h_1 = \sqrt{x_\xi^2 + y_\xi^2}, \qquad h_2 = \sqrt{x_\eta^2 + y_\eta^2}, \quad (9)$$

and $\hat{U}$ and $\hat{V}$ are given as

$$\hat{U} = \frac{1}{J}\left(h_2 u_1 - \frac{h_3}{h_1} v_1\right),$$

$$\hat{V} = \frac{1}{J}\left(h_1 v_1 - \frac{h_3}{h_2} u_1\right), \quad (10)$$

where $h_3 = y_\xi y_\eta + x_\xi x_\eta$; in (1)–(4) θ is the potential temperature, f is the Coriolis parameter, g is the gravitational acceleration, K_m is the vertical eddy viscosity coefficient, and K_h is the thermal vertical eddy friction coefficient. Here F_u, F_v, and F_θ represent the horizontal momentum and thermal diffusion terms, and ρ and ρ_o are the perturbation and reference densities, which satisfy $\rho_{\text{total}} = \rho + \rho_o$; F_u, F_v, and F_θ were calculated by Smagorinsky's formula (1963) in which the horizontal diffusion is directly proportional to the product of horizontal grid sizes. The coefficients K_m and K_h were calculated using the modified Mellor and Yamada level 2.5 turbulent closure scheme (Mellor and Yamada 1974, 1982; Galperin et al. 1988).

The surface and bottom boundary conditions for the momentum and heat equations are given by

$$\frac{\rho_0 K_m}{D}\left(\frac{\partial u_1}{\partial \sigma}, \frac{\partial v_1}{\partial \sigma}\right) = (\tau_{0\xi}, \tau_{0\eta}); \qquad \frac{\partial \theta}{\partial \sigma} = 0;$$

$$\omega = 0 \quad \text{at } \sigma = 0,$$

$$\frac{\rho_0 K_m}{D}\left(\frac{\partial u_1}{\partial \theta}, \frac{\partial v_1}{\partial \theta}\right) = (\tau_{b\xi}, \tau_{b\eta}); \qquad \frac{\partial \theta}{\partial \sigma} = 0;$$

$$\omega = 0 \quad \text{at } \sigma = -1,$$

where $(\tau_{0\xi}, \tau_{0\eta})$ and $(\tau_{b\xi}, \tau_{b\eta}) = C_d\sqrt{u_1^2 + v_1^2}(u_1^2 + v_1^2)$ are the ξ and η components of surface wind and bottom stresses. The surface wind stress was calculated based on the neutral steady-state drag coefficient developed by Large and Pond (1981). The drag coefficient C_d at the bottom was determined by matching a logarithmic bottom layer to the model at a height z_{ab} above the bottom; that is,

$$C_d = \max\left[k^2/\ln\left(\frac{z_{ab}}{z_0}\right)^2, 0.0025\right],$$

where $k = 0.4$ is the von Kármán constant and z_0 is the bottom roughness parameter, which was taken as 0.001 m in this study. The lateral boundary condition for closed basins such as the Great Lakes is specified as $v_n = 0$, where v_n is the normal velocity component at the boundary.

The numerical domain covered the entire volume of Lake Superior with higher resolution near the Keweenaw Peninsula coast. The horizontal grids were almost orthogonal in the interior lake but nonorthogonal along the Keweenaw coast. Total grid points (including dry points on land that were not used in numerical computation) are 126 (alongshelf) $\times$ 109 (cross-shelf). Along the Keweenaw coast, the horizontal grid resolution was about 2–4 km in the cross-shelf direction and about 4–6 km in the alongshelf direction. Thirty-one uniform σ levels were used in the vertical, which resulted in a vertical resolution of about 1 m near the coast and 10 m at the 300-m isobath in the interior. The time step of the numerical integration was 360 s.

To examine the physical processes that control the formation and evolution of the thermal front and Keweenaw Current, several numerical experiments were conducted for the cases with summertime stratification. First, the model was run as a Rossby adjustment problem for a given initial temperature field and initial zero fields of u_1, v_1, and ζ. It was then run prognostically with idealized wind forcings. To examine the physical mechanism driving the baroclinic instability of the thermal front and eddy formation, the evolution of temperature and current fields were also tracked by running the model without atmospheric forcing.

The initial temperature field was interpolated directly from the regional hydrographic data obtained in June and September 1973 (Figs. 2 and 3), respectively, by the Canadian Center for Inland Waters (International Joint Commission 1977). The spatial resolution of temperature observations was about 10 km. The June and September 1973 temperature fields represented the early and late summer stratification cases. In June 1973, a significant cross-shelf temperature gradient occurred only along the southern side of the lake. A thermal front was evident along the southern coast, with a surface water temperature of about 10°C along the Keweenaw Peninsula and 4°C approximately 20 km away from the coast. The vertical scale of the thermal front was about 60 m. In September 1973, the temperature field was characterized by a warm interior and a wider thermal front along the coast. The surface water temperature was about 16°C at the coast along the Keweenaw Peninsula

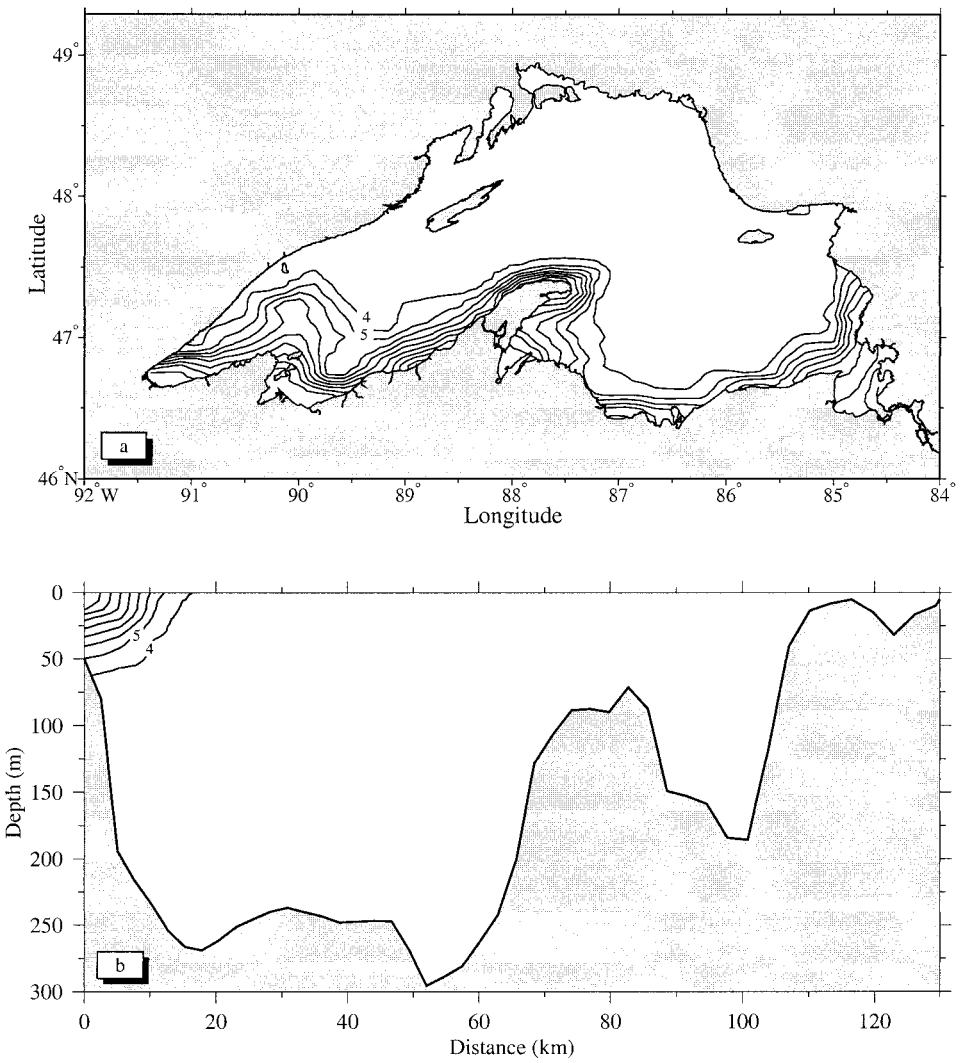

FIG. 2. Initial surface and cross-shelf distributions of temperature for the Jun 1973 stratification case. The temperature at each grid point was interpolated directly from the regional hydrographic dataset taken in June 1973 in Lake Superior.

and decreased to 10°C over a cross-shelf distance of about 35 km. Strong vertical stratification occurred in the upper 100 m.

3. Model results

a. Density-driven current

Without atmospheric forcing, the cross-shelf temperature gradient tended to create a well-defined alongshelf coastal current jet along the Keweenaw Peninsula for both the June and September 1973 cases (Figs. 4 and 5). This current jet formed within an inertial period of 16.4 h after the Rossby adjustment of the current field to the initial temperature field. The magnitude and spatial scale of the jet depended on the initial cross-shelf temperature gradients and vertical stratification. In June 1973, the model predicted a narrow alongshelf current with a cross-shelf scale of 12 km and a vertical scale of 20 m. The maximum current, about 10 cm s^{-1}, occurred about 5 km from the coast where the cross-shelf temperature gradient was largest. In September 1973, the model-predicted, alongshelf current jet intensified significantly, then shifted offshore and extended to deeper levels. The cross-shelf scale of the jet was about 30 km, with a maximum current of 15 cm s^{-1}, 10 km from the coast. The vertical scale of the jet was about 40 m, twice as thick as that which occurred in June 1973.

The model also predicted a baroclinic cyclonic circulation around Lake Superior in the summer of 1973. In June, this circulation was mainly restricted to the southern coast where the cross-shelf temperature gradient was significant. A closed cyclonic circulation existed in September. The water moved fast along the southern coast, and then less rapidly recirculated cy-

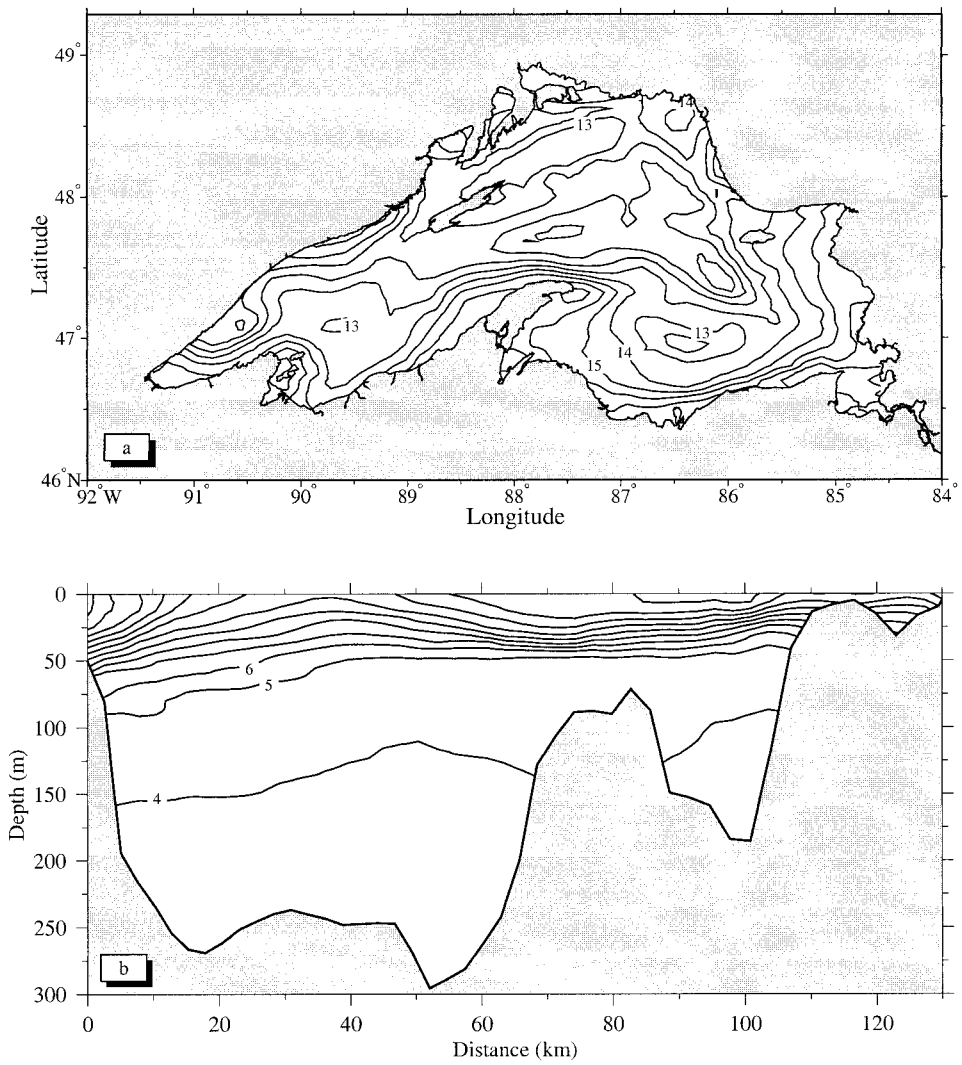

FIG. 3. Initial surface and cross-shelf distributions of temperature for the Sep 1973 stratification case. The temperature at each grid point was interpolated directly from the regional hydrographic dataset taken in Sep 1973 in Lake Superior.

clonically around the eastern, northern, and western coasts.

The model-predicted, density-driven flow in the Rossby adjustment problem represented only a baroclinic component of the Keweenaw Current. No mechanism was present to create a barotropic component, which can be seen in the vertical distribution of the current, where a relatively weak, westward return flow occurred below the eastward coastal jet. In September 1973, the model predicted a westward flow at the surface in the upstream region of the Keweenaw Current, which was likely to be a density-driven recirculation as the thermal front shifted offshore. This recirculation, however, could be the result of an extrapolation uncertainty in the initial temperature field since the number of temperature samples acquired near the coast in September 1973 was not sufficient to resolve this feature.

The speed of the model-predicted, density-driven alongshelf current jet in June and September 1973 varied in the range of 10 to 15 cm s^{-1}, which was about a third of the speed observed Keweenaw Current in July 1973 (Niebauer et al. 1977). This result suggests that the buoyancy force associated with the thermal front was not the only factor that controlled the Keweenaw Current. Hence both barotropic and baroclinic responses of the current to the surface wind must also be crucial in the formation, evolution, and perturbation of the Keweenaw Current. A detailed discussion of the effect of wind-forcing follows.

b. Effects of winds

During the summer of 1973, the atmosphere over Lake Superior was dominated by northward winds and

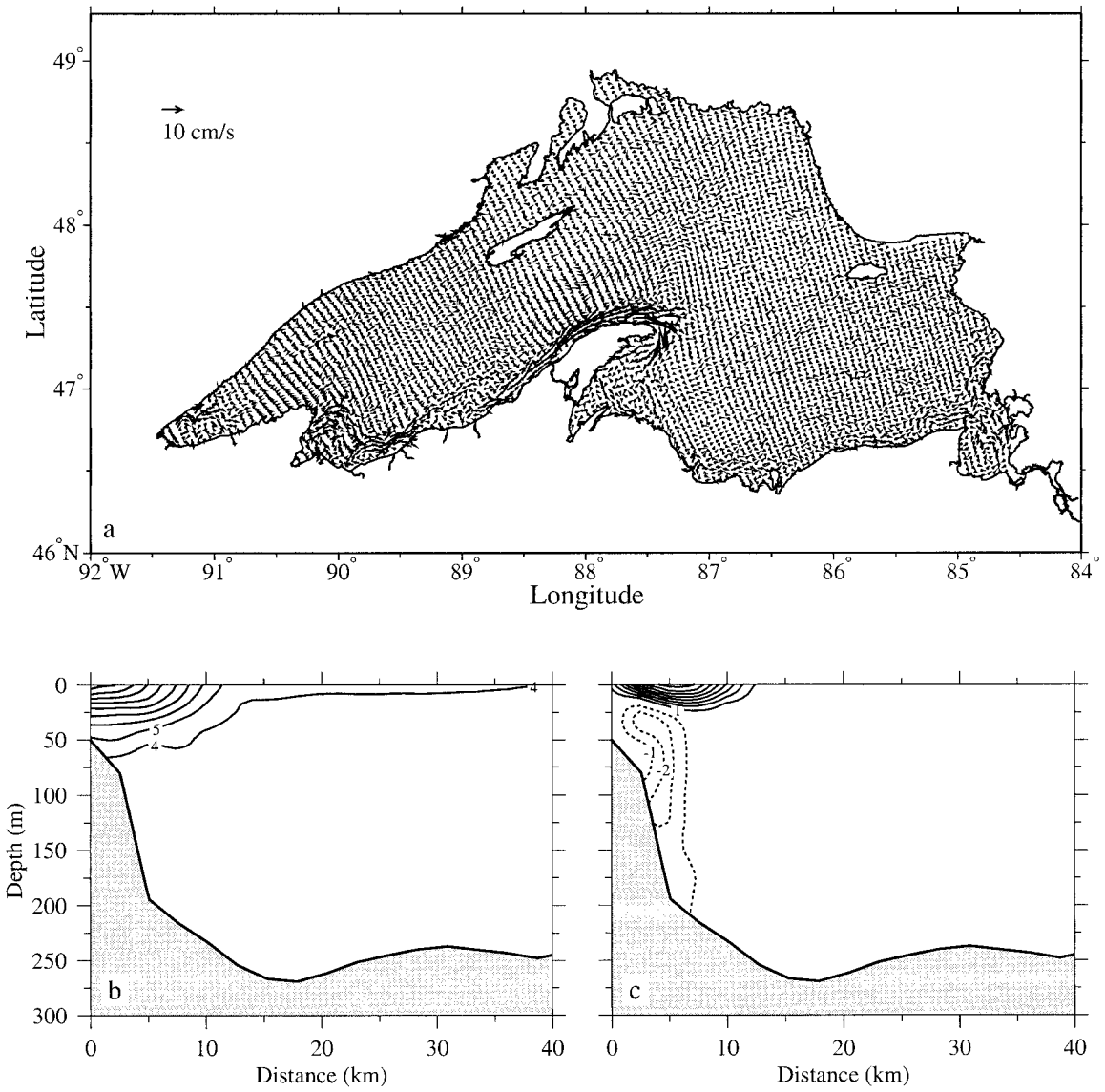

FIG. 4. Surface distribution of current vectors (a) and cross-shelf distributions of temperature (b) and alongshelf velocity (c) at the end of the first model day for the Jun 1973 stratification case.

atmospheric frontal passages with a timescale of about 5 days (Phillips 1978). To examine the response of the Keweenaw Current to atmospheric forcing, we added wind forcing to the previously described model run after the first model day when the density-driven flow was established. Four cases were conducted for: 1) northeastward (NE), 2) southeastward (SE), 3) northwestward (NW), and 4) southwestward (SW) winds. In all of these, the wind speed was taken as a constant of 5 m s^{-1}.

The spatial distributions of temperature and current at the surface and on section 1 at the end of the fifth model day for the September stratification are examined (Figs. 6 and 7). The northeastward wind tended to produce an onshore Ekman transport near the surface, which displaced the thermal front toward the coast. As a result, the eastward, alongshelf current accelerated dramatically near the coast, and the maximum speed exceeded 20 m s^{-1}. The wind-induced onshore Ekman flow led to a remarkable downwelling along the slope. This downwelling tended to advect the isotherms downward and caused a narrow eastward flow near the coast. In this case, the cross-shelf scale of the Keweenaw Current shrank to about 10 km, which was a factor of 2 smaller than that resulting from the initial condition.

The southeastward wind produced a southwestward Ekman transport near the surface. As a result, the Keweenaw Current was dramatically reduced or reversed due to the cancellation of wind- and buoyancy-induced flows, even though there was still a significant cross-shelf temperature gradient near the coast. An upwelling

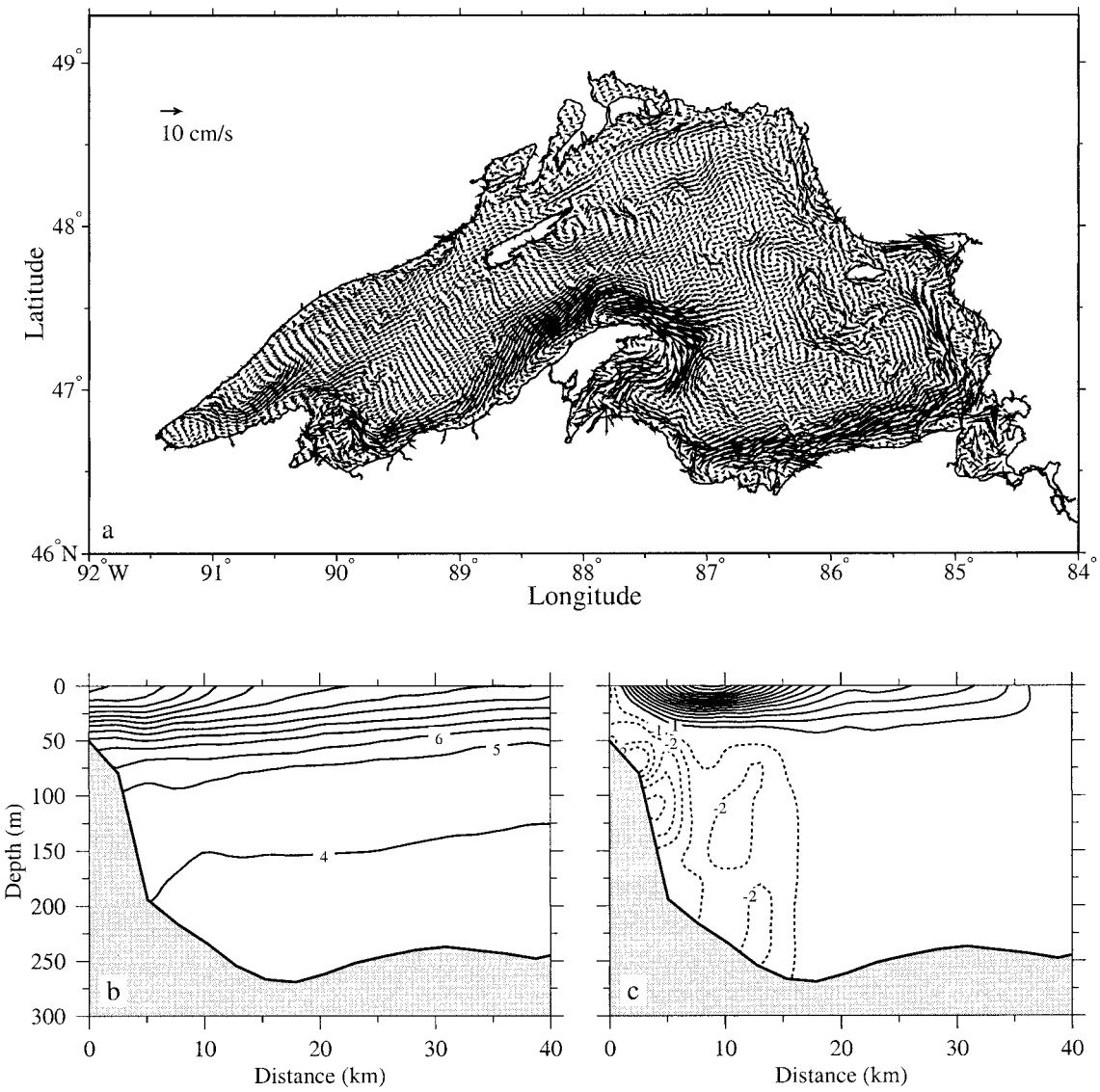

FIG. 5. Surface distribution of current vectors (a) and cross-shelf distributions of temperature (b) and alongshelf velocity (c) at the end of the first model day for the Sep 1973 stratification case.

was observed along the deep slope on section 1 (Fig. 1) where the surface alongshelf current was westward. A noticeable upwelling also was found near the bottom around the 60-m isobath, consistent with an upward shift of the 6°C isothermal line there.

The northwestward wind produced a northeastward near-surface Ekman transport, which pushed the isotherms away from the Keweenaw coast and hence significantly reduced the cross-shelf temperature gradient. Correspondingly, the eastward current jet weakened dramatically, and a weak clockwise recirculation formed near the coast. The offshore Ekman transport resulted in a noticeable upwelling along the slope at the coast.

The constant southwestward wind tended to push the isotherms northwestward, reversing the sign of the cross-shelf temperature gradient near the coast. A relatively strong westward current jet could form near the coast as a result of the combined effect of wind and density forcings. This current was about the same order of magnitude as the eastward Keweenaw Current, but its direction was reversed. In this case, the cross-shelf, secondary circulation was characterized by upwelling along the slope near the coast and downwelling at the near-surface convergence zone about 15 km away from the coast.

These model experiments suggest that the spatial distribution and magnitude of the Keweenaw Current were dramatically influenced by wind forcing. The eastward, alongshelf current tended to be retarded or reversed during an upwelling-favorable (northwestward or southwestward) wind but was not always enhanced during a downwelling-favorable wind. The model did show a

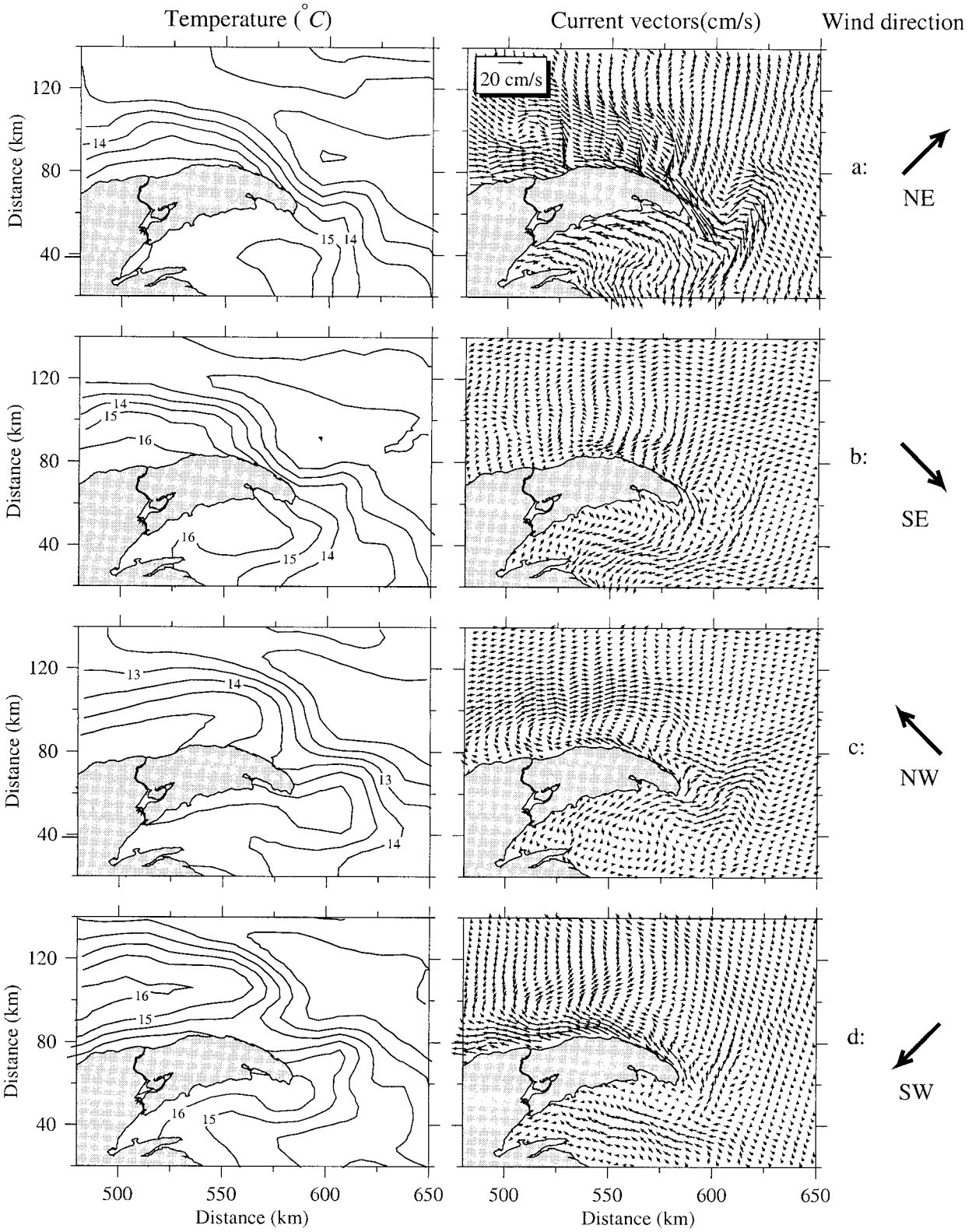

FIG. 6. Surface distributions of (left) temperature and (right) current vectors at the end of the fifth model day under (a) northeastward, (b) southeastward, (c) northwestward, and (d) southwestward wind conditions for the Sep 1973 stratification case.

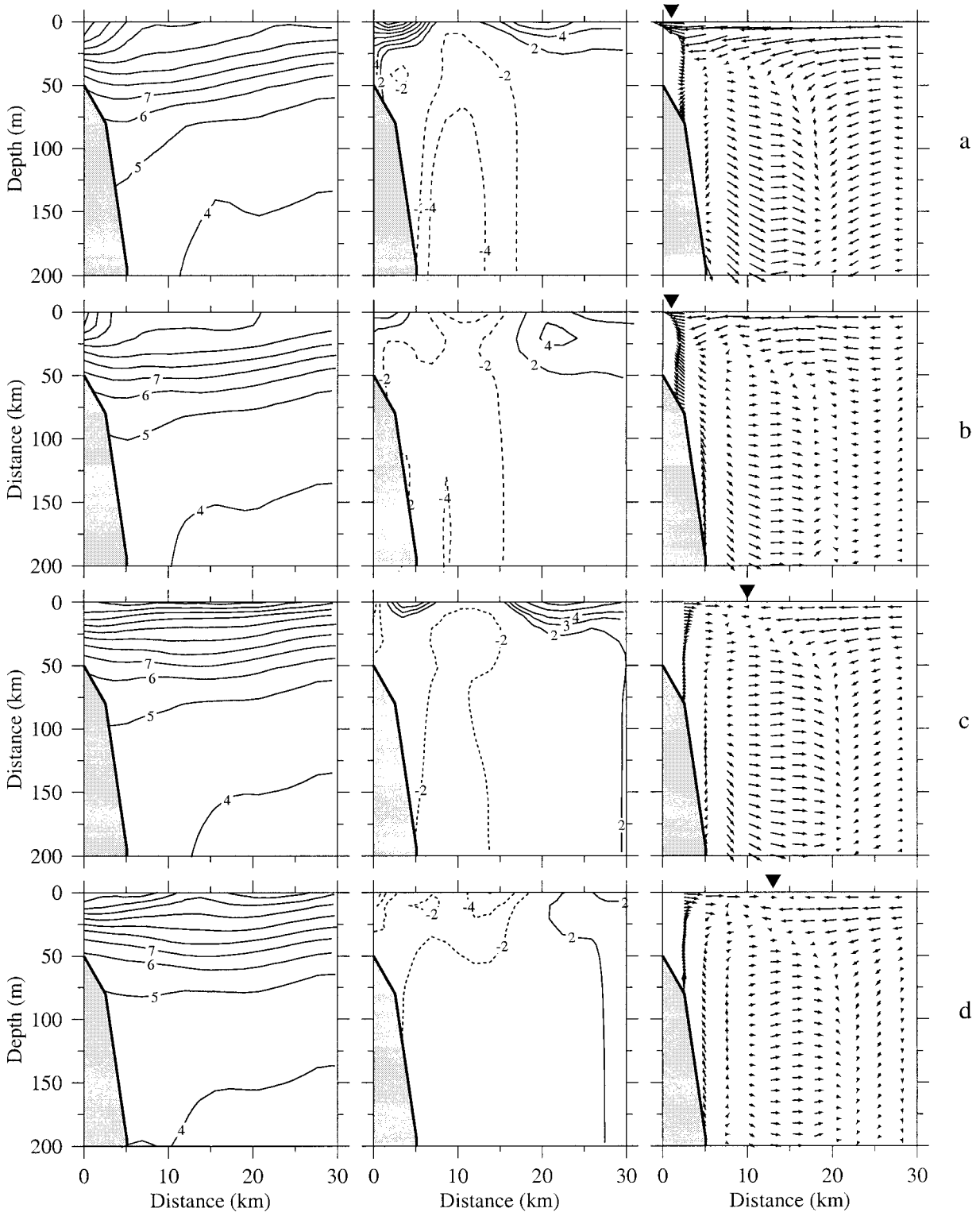

FIG. 7. Cross-shelf distributions of (left) temperature, (middle) alongshelf velocity, and (right) cross-shelf current vectors at the end of the fifth model day under (a) northeastward, (b) southeastward, (c) northwestward, and (d) southwestward wind conditions for the Sep 1973 stratification case.

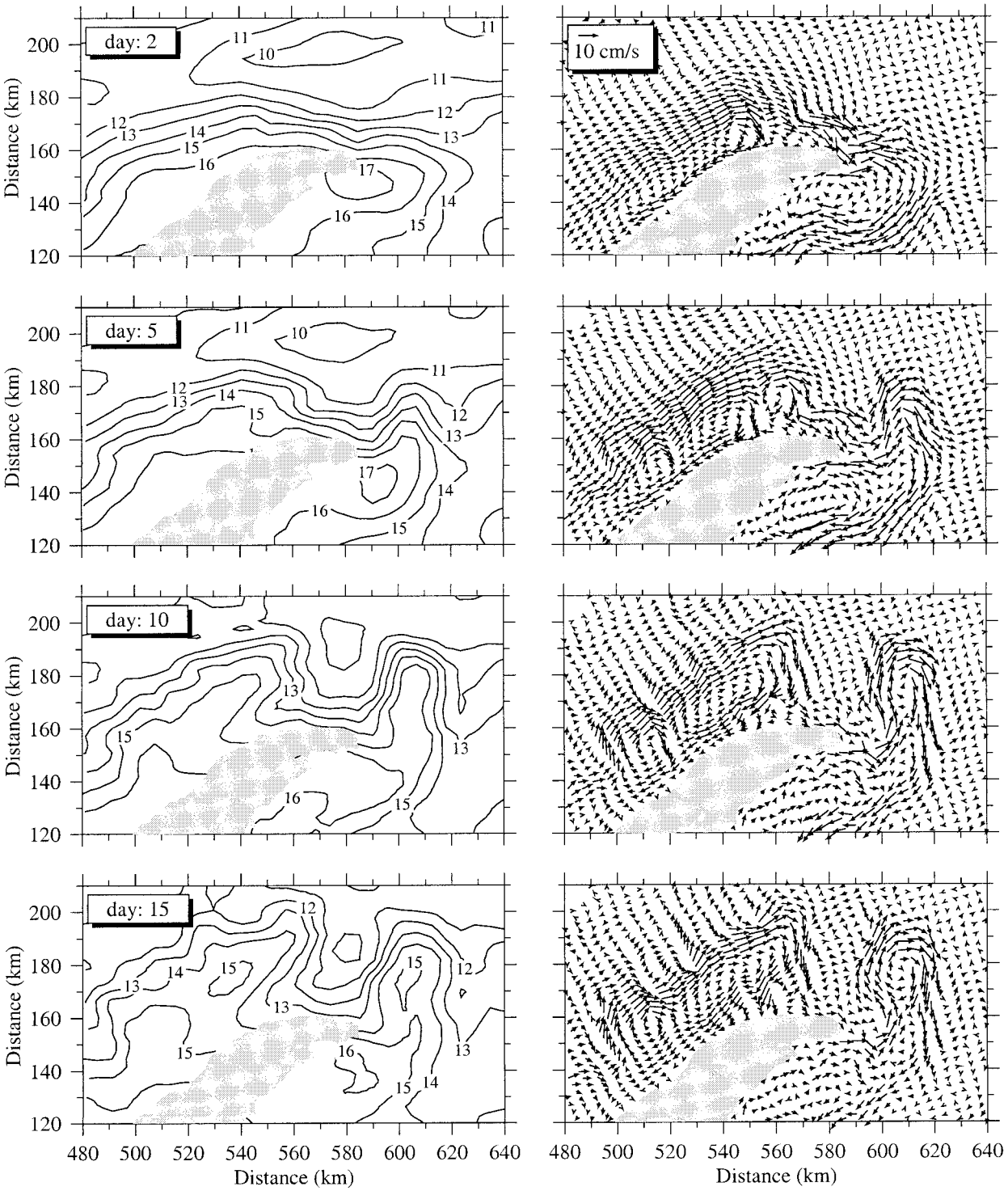

FIG. 8. Surface distributions of (left) temperature and (right) current vectors at model days 2, 5, 10, and 15 for the case without wind-forcing. The initial temperature field was the same as that shown in Fig. 3.

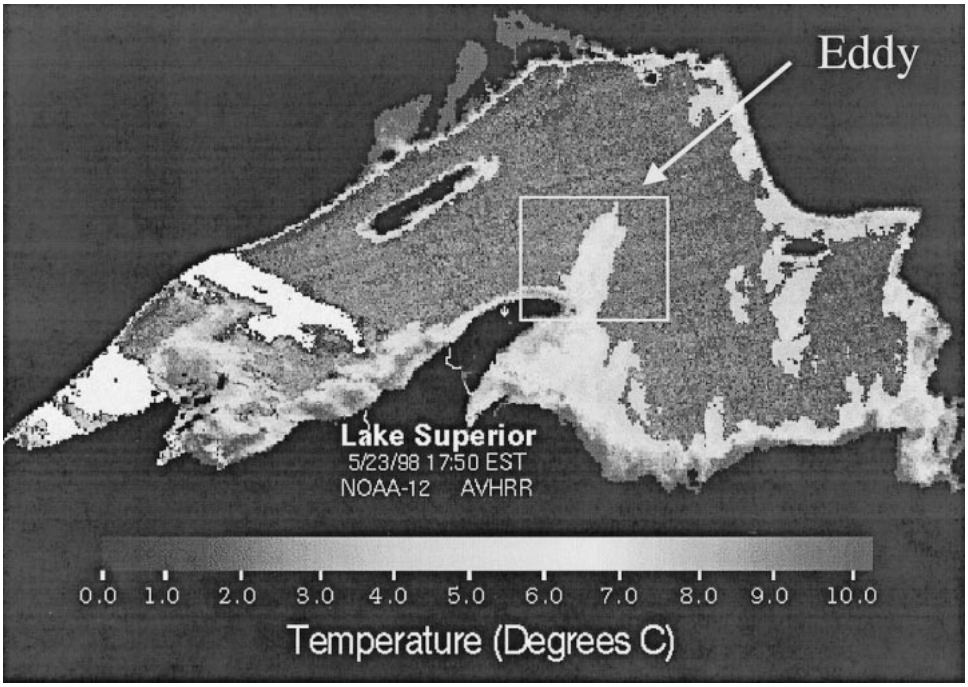

FIG. 9. The NOAA AVHRR satellite surface temperature image taken at 1750 EST 23 May 1998. The warm core shown in the box was an indicator of an eddy.

significant intensification of the Keweenaw Current during the northeastward wind but not during the southeastward wind. Although both northeastward and southeastward winds produced downwelling near the coast, the wind-induced barotropic water transport tended to cancel the buoyancy-induced current when a southeastward wind was present. These model experiments also suggest that an accurate and frequent measurement of wind speed and direction along the Keweenaw Peninsula is needed for prediction of the Keweenaw Current.

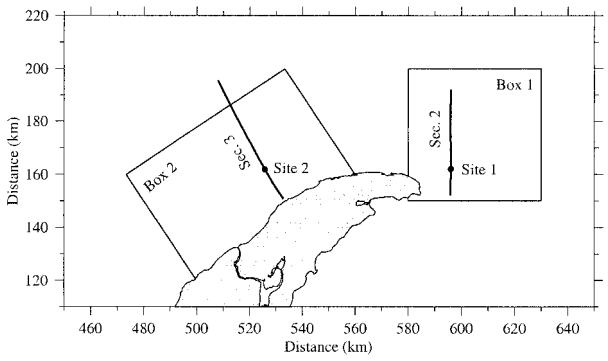

FIG. 10. The investigation domains used for the energy budget analysis. Solid lines indicate the sections used to calculate the barotropic component of the cross-shelf gradient of potential vorticity, and filled dots represent the sites used to calculate the baroclinic component of the cross-shelf gradient of potential vorticity. Boxes 1 and 2 are the areas used to estimate the energy budget.

c. Eddy formation

To examine the instability of the thermal front near the Keweenaw coast, the model was run prognostically without atmospheric forcing for the case with September 1973 stratification. As mentioned above, a well-defined coastal current jet was established on the first model day as a result of the adjustment of the current field to the temperature field (Fig. 5). Once the coastal current jet formed, however, the thermal front started to migrate offshore in the upstream region and around the head of the Keweenaw Peninsula. As a result, a warm-core eddy, characterized by an anticyclonic circulation, formed offshore on the eastern side of the Keweenaw Peninsula, and a clockwise recirculation occurred along the Keweenaw coast (Fig. 8). The model-predicted warm-core eddy had a radius of about 13 km and a maximum swirl speed of about 13 cm s^{-1}. The location and shape of this eddy coincided well with the satellite surface temperature (SST) image for 23 May 1998 (Fig. 9). A similar evolution pattern of temperature and current field was also found in the June 1973 stratification case after the wind relaxed. This result supports the notion that the model-predicted warm-core eddy probably represented a general summertime dynamic feature on the eastern side of the peninsula.

4. Instability of the thermal front

What caused the formation of a warm-core eddy on the eastern side of the Keweenaw Peninsula? To address

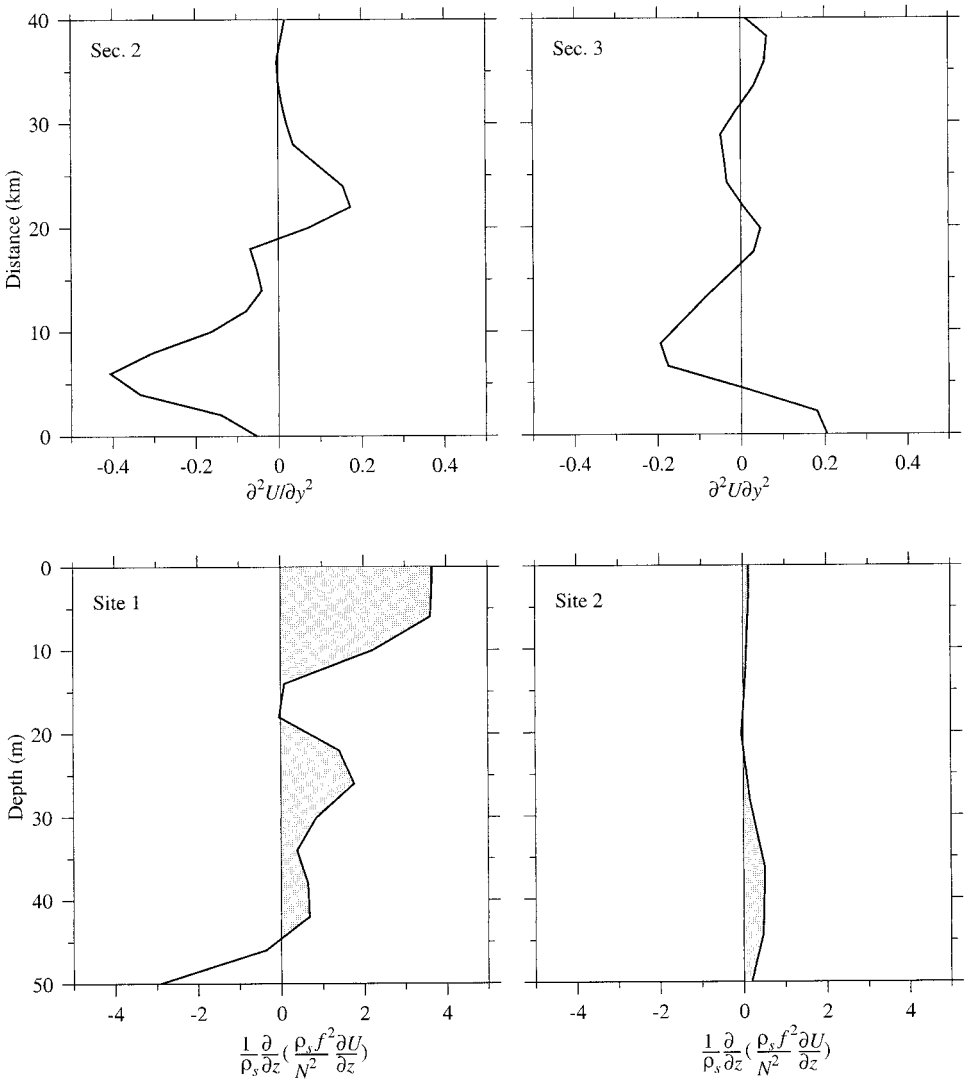

FIG. 11. Distributions of the barotropic and baroclinic components of potential vorticity at the end of the first model day on sections (left) 2 and (right) 3 and sites (left) 1 and (right) 2 shown in Fig. 10.

this question, we examined both the barotropic and baroclinic instabilities of the coastal current jet. The momentum analysis suggests that the model-predicted, alongshelf current was dominantly quasigeostrophic. The necessary condition for instability is that the potential vorticity gradient in the cross-stream direction changes sign somewhere in the flow (Pedlosky 1979). In the barotropic case, where the current varies only with cross-shelf direction, that is, $U = U(t, y)$, the necessary condition for instability of a jet is

$$\frac{\partial^2 U}{\partial y^2} = 0, \tag{11}$$

while for the baroclinic case, where $U = U(t, z)$, the necessary instability condition on an f plane becomes

$$\frac{1}{\rho_s}\frac{\partial}{\partial z}\left(\frac{\rho_s}{N^2}\frac{\partial U}{\partial z}\right) > 0, \tag{12}$$

where U is the alongshelf current, $\rho_s = \rho_s(z)$ is the reference density, N is the Väisälä frequency, and y and z are the cross-shelf and vertical axes of the coordinates, respectively. Here y is equivalent to η (Pedlosky 1979).

The left-side terms of both (11) and (12) were calculated on selected sections and at selected sites, respectively (Fig. 10). On both sections, the near-surface, cross-shelf gradient of potential vorticity changed sign across the current jet, which suggests that the current jet may become barotropically unstable along the Keweenaw coast (Fig. 11, upper panel). In the vertical, at reference sites in the center of the current jet, the left-side term of (12) was positive over most of the water

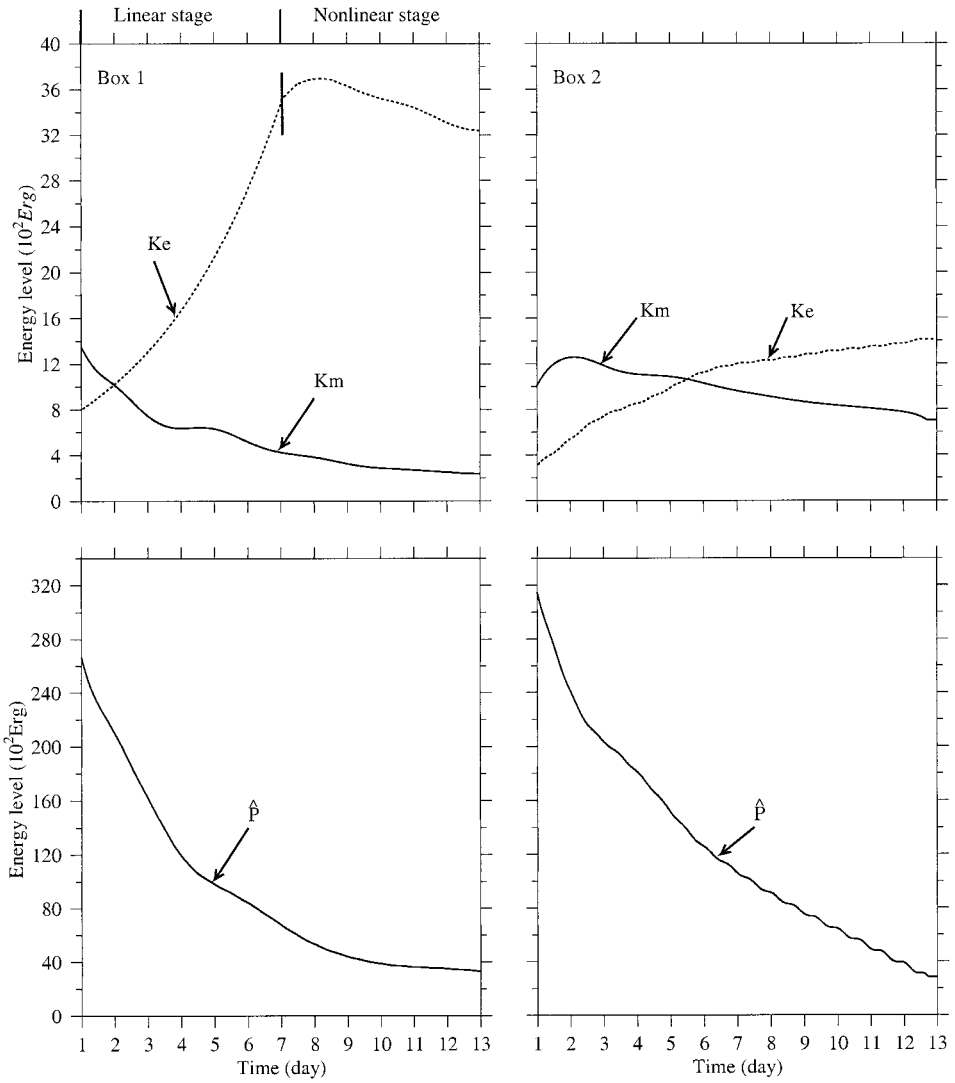

FIG. 12. Time evolution of the volume-averaged mean kinetic energy ($\mathcal{K}_m$), eddy kinetic energy ($\mathcal{K}_e$), and available potential energy ($\hat{\mathcal{P}}$) for boxes (left) 1 and (right) 2.

column (especially in the upper 15 m) on the eastern section and was positive (but had small magnitude) over all of the water column on the western section (Fig. 11, lower panel). This pattern suggests that the current was more baroclinically unstable near the head of the Keweenaw Peninsula than in the upstream region along the Keweenaw coast.

The instability analysis based on (11) and (12) suggests that the Keweenaw Current is unstable. Since these criteria only represent the necessary conditions for instability, however, it is not sufficient to make a conclusion that the anticyclonic warm-core eddy circulation found in both model and observations was a result of an instability of the Keweenaw Current; the evolution and transfer of the eddy kinetic energy in the jet must also be considered.

The equations for the volume-averaged, mean kinetic energy (MKE), eddy kinetic energy (EKE), and available potential energy (APE) are given as

$$\frac{\partial \mathcal{K}_e}{\partial t} = \langle \mathcal{K}_m, \mathcal{K}_e \rangle + \langle \mathcal{P}_e, \mathcal{K}_e \rangle + \text{advection of EKE} + \text{diffusion of EKE} \tag{13}$$

$$\frac{\partial \mathcal{K}_m}{\partial t} = \langle \mathcal{K}_m, \mathcal{K}_e \rangle + \langle \mathcal{P}_m, \mathcal{K}_m \rangle + \text{advection of MKE} + \text{diffusion of MKE} \tag{14}$$

$$\frac{\partial \hat{\mathcal{P}}}{\partial t} = -\langle \mathcal{P}_e, \mathcal{K}_e \rangle - \langle \mathcal{P}_m, \mathcal{K}_m \rangle + \text{advection of APE} + \text{diffusion of APE}, \tag{15}$$

where

$$(\mathcal{K}_e,\ \mathcal{K}_m,\ \hat{\mathcal{P}}) = \frac{1}{V_o}\int_0^{L_x}\int_0^{L_y}\int_{-h}^{\zeta} (\text{EKE, MKE, APE})\ dx\ dy\ dz; \quad \text{and}$$

$$\langle \mathcal{K}_m,\ \mathcal{K}_e\rangle = -\rho_o \int_0^{L_x}\int_0^{L_y}\int_{-h}^{\zeta}\left[\overline{v'u'}\frac{\partial \overline{u}}{\partial y} + \overline{w'u'}\frac{\partial \overline{u}}{\partial z} + \overline{v'v'}\frac{\partial \overline{v}}{\partial y} + \overline{w'v'}\frac{\partial \overline{v}}{\partial z}\right] dx\ dy\ dz,$$

$$\langle \mathcal{P}_e,\ \mathcal{K}_e\rangle = -\int_0^{L_x}\int_0^{L_y}\int_{-h}^{\zeta}\overline{\rho'w'}g\ dx\ dy\ dz; \qquad \langle \mathcal{P}_m,\ \mathcal{K}_m\rangle = -\int_0^{L_x}\int_0^{L_y}\int_{-h}^{\zeta}\overline{\rho}\,\overline{w}g\ dx\ dy\ dz,$$

where L_x, L_y, h, and V_o were the width, length, height, and volume of the investigation domain, and EKE, MKE, and APE were defined as

$$\text{EKE} = \frac{\rho_o}{2}(u'^2 + v'^2);$$

$$\text{MKE} = \frac{\rho_o}{2}(\overline{u}^2 + \overline{v}^2), \quad \text{and}$$

$$\text{APE} = (\rho(t) - \rho(o))gz,$$

and overbar and prime denote the along-jet averaged and perturbation components of a variable, respectively. The along-jet direction was defined as the streamline of the current jet at the end of the first model day before the temperature field started to evolve. The x and y coordinates were defined as the along- and cross-jet axes. For example,

$$\overline{u}(y, z, t) = \frac{1}{L_x}\int_0^{L_x} u(x, y, z, t)\ dx;$$

$$u'(x, y, z, t) = u(x, y, z, t) - \overline{u}(y, z, t).$$

Equations (13)–(15) indicate that the growth of the eddy kinetic energy depends on the energy conversion from the mean kinetic energy $\langle \mathcal{K}_m, \mathcal{K}_e\rangle$, and the eddy potential energy $\langle \mathcal{P}_e, \mathcal{K}_e\rangle$, the net flux of the eddy kinetic energy into the box with a volume of V_o, and turbulent diffusion. If horizontal and vertical diffusions are neglected, the total energy is conserved in the box.

Figure 12 shows the time evolution of mean kinetic energy ($\mathcal{K}_m$), eddy kinetic energy ($\mathcal{K}_e$), and available potential energy ($\hat{\mathcal{P}}$) averaged over a volume of V_o for boxes 1 and 2. In box 1, $\mathcal{K}_e$ grew exponentially during days 1–7, increased gradually during days 7–8, and decreased slowly thereafter. Correspondingly, $\hat{\mathcal{P}}$ decreased rapidly during days 1–7, and then tended to approach an equilibrium state after the 10th day. Here $\mathcal{K}_m$ decreased gradually during days 1–7, and, thereafter, tended to reach an equilibrium state as did $\hat{\mathcal{P}}$. The evolution of $\mathcal{K}_e$, $\mathcal{K}_m$, and $\hat{\mathcal{P}}$ was consistent with linear instability theory (Pedlosky 1979), which shows that instability develops as two stages: an initial linear stage followed by a nonlinear one. The eddy kinetic energy grows exponentially in the linear stage, and when the instability saturates, it then decreases gradually in the nonlinear stage. These two stages were clearly evident in box 1. The fact that the exponential growth of $\mathcal{K}_e$ was a result of the transfer of the available potential energy to eddy kinetic energy implies that the anticyclonic warm-core eddy found in box 1 was mainly caused by a baroclinic instability of the current jet.

Unlike the eastern coastal area of the Keweenaw Peninsula, in box 2, $\mathcal{K}_e$ grew gradually over time, along with a slow decrease of $\mathcal{K}_m$ and a rapid decrease of $\hat{\mathcal{P}}$, which suggests that the formation of an anticyclonic circulation in that area was the result of the advective and diffusive evolutions of temperature and current fields rather than baroclinic instability.

The energy budget was averaged over two stages in box 1 (Fig. 13). During the linear development stage, $\mathcal{K}_e$ increased at an average rate of 4.78×10^{-3} erg s^{-1}. The energy required for the rapid growth of $\mathcal{K}_e$ was supplied mainly by the transfer of the available eddy potential energy to the eddy kinetic energy [$\langle \mathcal{P}_e, \mathcal{K}_e\rangle = 5.34 \times 10^{-3}$ erg s^{-1}] against the energy loss due to turbulent diffusion (-1.38×10^{-3} erg s^{-1}). The transfer of the mean kinetic energy to the eddy kinetic energy $\langle \mathcal{K}_m, \mathcal{K}_e\rangle$ and an inward net flux of the eddy kinetic energy were 0.81×10^{-3} erg s^{-1} and 0.02×10^{-3} erg s^{-1}, respectively, which were only about 15% and 4% of $\langle \mathcal{P}_e, \mathcal{K}_e\rangle$, respectively. Again, this supported the conclusion that the eddy formation in box 1 was caused by the linear baroclinic instability of the current jet.

In the linear stage, the mean kinetic energy $\mathcal{K}_m$ was lost at an average rate of 1.61×10^{-3} erg s^{-1}. A large amount of the mean available potential energy (19.88×10^{-3} erg s^{-1}) was transferred to $\mathcal{K}_m$ through $\langle \mathcal{P}_m, \mathcal{K}_m\rangle$. This part of the energy, however, was not enough to compensate for the energy loss due to turbulent diffusion (20.41×10^{-3} erg s^{-1}), an outward net flux of the mean kinetic energy (0.28×10^{-3} erg s^{-1}), and the transfer to the eddy kinetic energy (0.81×10^{-3} erg s^{-1}). The available potential energy $\hat{\mathcal{P}}$ decreased rapidly at an average rate of 32.38×10^{-3} erg s^{-1}. The loss of $\hat{\mathcal{P}}$ was mainly transferred to $\mathcal{K}_m$ and $\mathcal{K}_e$ and advected to the surrounding region.

In the nonlinear stage, the temporal changes of $\mathcal{K}_e$, $\mathcal{K}_m$, and $\hat{\mathcal{P}}$ were controlled dominantly by a dissipation process at average loss rates of 1.01, 0.32, and 5.09×10^{-3} erg s^{-1}, respectively. In contrast to the linear stage,

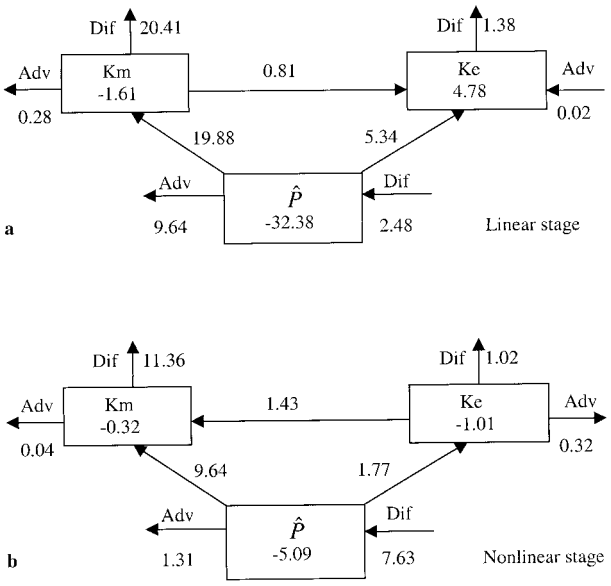

FIG. 13. Energy budget averaged over linear and nonlinear stages of the development of baroclinic instability for box 1. The values written below $\mathcal{K}_m$, $\mathcal{K}_e$, and $\hat{P}$ represent the net gain and loss rates of the energy per second. The values written near the arrows were the net transfers of energy from one to another. The unit is 10^{-3} erg s^{-1}.

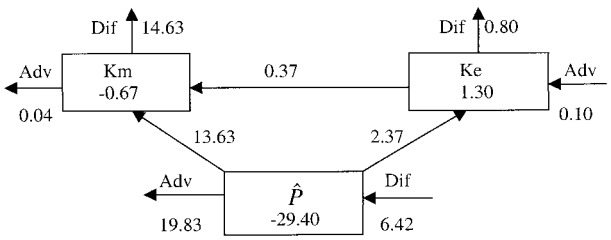

FIG. 14. Energy budget averaged over linear and nonlinear stages of the development of baroclinic instability for box 2. The values written below $\mathcal{K}_m$, $\mathcal{K}_e$, and $\hat{P}$ represent the net gain and loss rates of the energy per second. The values written nearby an arrow were the net transfers of energy from one to another. The unit is 10^{-3} erg s^{-1}.

a relatively large amount of $\mathcal{K}_e$ was transferred back to $\mathcal{K}_m$ ($\langle \mathcal{K}_m, \mathcal{K}_e \rangle = -1.43 \times 10^{-3}$ erg s^{-1}) and also advected out of the domain to the surrounding region (advection of EKE $= -0.32 \times 10^{-3}$ erg s^{-1}). Except for the term $\langle \mathcal{K}_m, \mathcal{K}_e \rangle$, the temporal change of $\mathcal{K}_m$ in this stage was very similar to that which occurred in the linear stage; $\mathcal{K}_m$ continued to decrease slowly, which was caused by turbulent dissipation against the energy transfers from mean available potential energy and eddy kinetic energy. The loss of $\mathcal{K}_m$ due to advection was 0.04×10^{-3} erg s^{-1}, only about 3.5% of the diffusion term. Compared to the linear stage, the temporal change of $\hat{P}$ became smaller. This result occurred because there was a decrease in the energy transfer to $\mathcal{K}_m$ and $\mathcal{K}_e$ and outward net advection, and an increase in the energy production due to turbulent diffusion.

The energy budget found in box 2 differed significantly from that found in box 1 (Fig. 14). The model showed a rapid decrease of $\hat{P}$ at an average rate of -29.4×10^{-3} erg s^{-1}. The major portion of this energy was transferred to $\mathcal{K}_m$ (-13.64×10^{-3} erg s^{-1}) and advected outward (-19.83×10^{-3} erg s^{-1}), with a compensation of 6.42×10^{-3} erg s^{-1} from turbulent diffusive flux. The transfer from $\hat{P}$ to $\mathcal{K}_e$, about -2.37×10^{-3} erg s^{-1}, plus the advection of EKE, directly caused $\mathcal{K}_e$ to increase slowly over time. Similar to the nonlinear stage in box 1, $\mathcal{K}_e$ was transferred to $\mathcal{K}_m$ ($\langle \mathcal{K}_m, \mathcal{K}_e \rangle = -0.37 \times 10^{-3}$ erg s^{-1}) and also diffused out of the domain at a rate of -0.8×10^{-3} erg s^{-1}. Gradually $\mathcal{K}_m$ decreased at an average rate of -0.67×10^{-3} erg s^{-1}. This decrease was balanced by the energy gain from $\langle \mathcal{P}_m, \mathcal{K}_m \rangle$ and the advection of EKE, as well as energy loss from outward advective and diffusive fluxes of MKE. The energy budget in box 2 supports the suggestion that the anticyclonic circulation found along the Keweenaw coast probably was a result of the gradual evolution of temperature and current fields through a slow adjustment process.

5. Summary

The formation and evolution of the Keweenaw Current in Lake Superior were examined using a nonorthogonal coordinate primitive equation numerical model developed by Chen et al. 1999, manuscript submitted to *J. Atmos. Oceanic Technol.*). The model was initialized by the monthly average temperature field observed in June and September 1973 and was run prognostically under different forcing conditions with and without winds. As a Rossby adjustment problem, the model predicted the formation of a well-defined coastal current jet within an inertial timescale of 16.4 h after the adjustment from an initial quiescent temperature field. The magnitude and direction of this current jet varied with the cross-shelf temperature gradient and winds. It tended to intensify during northeastward (downwelling favorable) winds, and to lessen or even reverse during northwestward to southwestward (upwelling favorable) or southeastward (downwelling favorable) winds.

In a case with strong stratification and without atmospheric forcing, a well-defined, warm-core eddy formed near the northeastern coast of the Keweenaw Peninsula as a result of baroclinic instability. A similar warm-core eddy was detected on 23 May 1998 from the Advanced Very High Resolution Radiometer surface temperature images, with the same shape, size, and location as the model-predicted eddy. The energy budget analysis suggested that the eddy developed during two stages: 1) rapid growth and 2) slow dissipation. The first stage was mainly characterized by the exponential growth of the eddy kinetic energy through a significant transfer from the available eddy potential energy. The second stage was controlled dominantly by a slow dissipation process of eddy and mean kinetic energies and available potential energy. During this stage, the decay of the eddy potential energy was mainly due to turbulent

diffusion, transfer to the mean kinetic energy, and outward net energy flux.

Process studies conducted by numerical simulation have provided insight into the formation and evolution of the Keweenaw Current under conditions of summertime stratification. The model experiments also suggest that the thermal front was gradually diffused over time without the input of external heating. What is the role of the solar heating in maintaining the strength of a thermal front? Is the model capable of simulating the Keweenaw Current? These questions have been addressed in Zhu et al. (2001) as Part II of our model experiments.

Acknowledgments. This research was supported by the National Science Foundation under Grants OCE-9712869 for Changsheng Chen, OCE-9712871 for Elise Ralph, and OCE-9712872 for Sarah Green and Judy Budd. We thank Georges Davidson for his editorial help. Two anonymous reviewers have provided many critical comments and constructive suggestions. Their help is greatly appreciated.

REFERENCES

Bennett, E. B., 1978: Characteristics of the thermal regime of Lake Superior. *J. Great Lakes Res.,* **4,** 310–319.

Blumberg, A. F., 1994: A primer for ECON-si. Tech. Report, HydroQual, Inc., Mahwah, NJ, 66 pp.

——, and G. L. Mellor, 1987: A description of a three-dimensional coastal ocean circulation model. *Three-Dimensional Coastal Models*, N. Heaps, Ed., Coastal and Estuarine Sciences Ser., Vol. 5, Amer. Geophys. Union, 1–6.

Chen, C., L. Zheng, and J. Zhu, 1999. A non-orthogonal primitive equation coastal ocean circulation model. *J. Atmos. Oceanic Technol.,* submitted.

Diehl, S., W. Maanum, T. Jordan, and M. Sydor, 1977: Transports in Lake Superior. *J. Geophys. Res.,* **82,** 977–978.

Galperin, B., L. H. Kantha, S. Hassid, and A. Rosati, 1988: A quasi-equilibrium turbulent energy model for geophysical flows. *J. Atmos. Sci.,* **45,** 55–62.

Green, T., and L. A. Yeske, 1974: Surface kinetic energy transfers in the Keweenaw Current. Contribution No. 24, Marine Studies Center, University of Wisconsin, 50 pp.

International Joint Commission, Upper Lakes Reference Group, 1977: *The Waters of Lake Huron and Lake Superior*. Vol. III, Parts A and B.

Lam, D. C., 1978: Simulation of water circulations and chloride transports in Lake Superior for summer 1973. *J. Great Lakes Res.*, **4,** 343–349.

Large, W. S., and S. Pond, 1981: Open ocean momentum flux measurements in moderate to strong winds. *J. Phys. Oceanogr.,* **11,** 324–406.

Matheson, D. H., and M. Munawar, 1978: Lake Superior basin and its development. *J. Great Lakes Res.,* **4,** 249–263.

Mellor, G. L., and T. Yamada, 1974: A hierarchy of turbulence closure models for planetary boundary layers. *J. Atmos. Sci.,* **31,** 1791–1896.

——, and ——, 1982: Development of a turbulence closure model for geophysical fluid problem. *Rev. Geophys. Space Phys.,* **20,** 851–875.

Niebauer, H. J., T. Green, and R. A. Ragotzkie, 1977: Coastal upwelling/downwelling cycles in southern Lake Superior. *J. Phys. Oceanogr.,* **7,** 918–927.

Pedlosky, J., 1979: *Geophysical Fluid Dynamics*. Springer-Verlag, 624 pp.

Phillips, D. W., 1978: Environmental climatology of Lake Superior. *J. Great Lakes Res.,* **4,** 288–309.

Smagorinsky, J., 1963: General circulation experiments with the primitive equations. I: The basic experiments. *Mon. Wea. Rev.*, **91,** 99–164.

Yeske, L. A., and T. Green, 1975: Short-term variations in a great lake coastal current by aerial photogrammetry. *J. Phys. Oceanogr.,* **5,** 125–135.

Zhu, J., C. Chen, E. Ralph, S. A. Green, J. Wells Budd, and F. Y. Zhang, 2001: Prognostic modeling studies of the Keweenaw Current in Lake Superior. Part II: Simulation, *J. Phys. Oceanogr.*, **31,** 396–410.